Eur. Phys. J. D **38**, 219–223 (2006)
DOI: 10.1140/epjd/e2006-00028-0

THE EUROPEAN PHYSICAL JOURNAL D

Characterization of an oriented metastable atom source based on a magnetic hexapole

D. Watanabe, H. Ohoyama[a], T. Matsumura, and T. Kasai

Department of Chemistry, Graduate School of Science, Osaka University Toyonaka, Osaka 560-0043, Japan

Received 2nd August 2005 / Received in final form 18 November 2005
Published online 8 February 2006 –

Abstract. The M_J-state selection of the metastable rare-gas (Rg*) was achieved by a magnetic hexapole that is composed of permanent magnets. The performance of the magnetic hexapole was examined by characterizing the velocity distribution and the spatial profile of the state selected Rg* beam. The characterization was carried out using position resolved time-of-flight analysis and its trajectory simulation. The magnetic hexapole enhanced the beam intensity at least one order of magnitude owing to the focusing effect. In addition, the magnetic hexapole was found to act as a good velocity selector.

PACS. 39.10.+j Atomic and molecular beam sources and techniques

1 Introduction

In general, the mutual orientation between two reactants should play an important role for their reaction, because their interaction potential will significantly depend on mutual orientation. Since the metastable rare-gas atoms have an open-shell electronic structure, $np^5(n+1)s^1$, the intermolecular interaction should depend not only on the molecular orientation but also on the magnetic sub level M_J of the rare-gas atoms. From this point of view, the reactions of metastable rare-gas atoms with small molecules are expected to depend on both the molecular orientation and the atomic orbital orientation. The steric effects on the molecular orientation have been studied in our laboratory using an electrostatic hexapole [1–5]. However, the steric effect on the atomic orbital orientation is still an unresolved problem. Recently, in order to ascertain the existence of steric effects on atomic orbital orientation, we studied the M_J-state- and the collision energy-dependence of the total attenuation cross-section for the Ar (^{3}P) + CF_3Br collision under the beam-cell condition by means of the M_J-state analysis of the survived Ar (^{3}P) after the collision with CF_3Br using a Stern-Gerlach type inhomogeneous magnet [6]. Although a significant M_J-state dependence was observed, the detail of the M_J selectivity could not been clarified, because the M_J-state selection before the collision process was not prepared in the previous study. For the quantitative understanding on the selectivity of M_J, there is no doubt that the preparation of the oriented Rg (^{3}P) beam before the collision is necessary.

For the metastable rare-gas atom production of spin-polarized Ne* by means of excitation using polarized light has been reported [7]. After the discovery of the atomic spin by Stern and Gerlach [8], the inhomogeneous magnetic field has been also used to produce spin polarized atomic beams. A magnetic hexapole field is also one of the techniques for generating spin-polarized atoms, and has been used to produce a low velocity metastable He beam [9].

The combination of the oriented molecular beam and the oriented Rg* beam will provide a powerful tool to resolve the steric effect on the reaction of the metastable rare-gas atom. In order to prepare the oriented metastable rare-gas (Rg*) beam for the advanced experimental studies in gas phase and surface molecular reaction dynamics, we constructed an oriented Rg* beam source based on a magnetic hexapole. In the present study, the performance of the magnetic hexapole was examined by characterizing the velocity distribution and the spatial profile of the state selected Rg* beam.

2 Experiment

2.1 Experimental set-up

A schematic view of the experimental set-up is shown in Figure 1. An inset in Figure 1 indicates the cross-sectional view of the magnetic hexapole. The magnetic hexapole is composed of unit magnetic hexapoles linked each other with a space gap of 5 mm. The total length of the magnetic hexapole field can be increased up to 8 units. The unit magnetic hexapole is a 40 mm-long magnetic hexapole piece constructed of the six permanent magnets (neodymium magnet, $40 \times 12 \times 5$ mm, the magnetic flux density on the surface is 3800 Gauss). The construction of the magnetic hexapole units was based on the report

[a] e-mail: ohyama@chem.sci.osaka-u.ac.jp

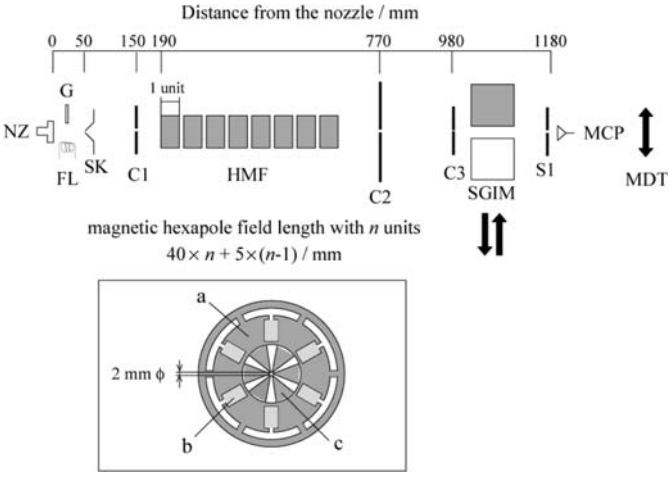

Fig. 1. A schematic drawing of the experimental set-up. NZ: pulsed valve, F: filament, G: grid, SK: skimmer 3 mm ϕ, C1: collimator 1.5 mm ϕ, C2: collimator 2 mm ϕ, C3: collimator 0.3 mm ϕ, S1: vertical slit with the width of 0.3 mm, MHF: magnetic hexapole field composed of the 40 mm-long magnetic hexapole units with six permanent magnets, SGIM: Stern-Gerlach type inhomogeneous magnet, MDT: motor driven translator, MCP: micro-channel plate detector. (Inset) Cross-sectional view of the magnetic hexapole; a: mild steel yoke, b: permanent magnet, c: pole piece.

by Jardine et al. [10] with some modifications, such as the diameter of unit, size of pole piece. The performance of this magnetic hexapole was examined by characterizing the velocity distribution and the spatial profile of the state selected metastable rare-gas (Rg*) beam. In the present study, He (^{3}S) and Ar ($^3P_2$) were used to characterize the newly developed magnetic hexapole. A beam of metastable He (^{3}S) and Ar ($^3P_2$) atoms was produced by a pulsed glow discharge with a pulse width of 5 and 10 μs, respectively. The discharge was ignited by applying the pulsed grid voltage, which served also as the time origin for the time-of-flight measurement with a flight length of 1.18 m. The focusing condition was changed by changing the total length of the magnetic hexapole field. The M_J- and velocity-selected Rg* beam by the magnetic hexapole field entered into a main chamber through a 2 mm ϕ collimator (C2). In this chamber, the velocity distribution and the spatial profile of the focused Rg* beam were measured using position resolved time-of-flight analysis. This analysis is accomplished by detecting Rg* on a MCP detector through a vertical slit of 0.3 mm width (S1) which position was scanned with a step of 0.12 mm by a motor driven translator. In order to identify of the M_J state of the focused beam (especially for Ar ($^3P_2$)), a Stern-Gerlach type inhomogeneous magnet (SGIM), which was equipped with a collimator of 0.3 mm ϕ (C3), was set after the state selection by the magnetic hexapole. From the direction and the magnitude of the deflection of Rg* by the SGIM, the M_J state experimentally identifies. The SGIM was operated by a 40 ms width pulsed current and was activated before the initiation of the glow discharge. In the present discharge condition, the additional species such as He (^{1}S) and Ar ($^3P_0$), which are inactive to the magnetic hexapole, coexist as a direct beam. The contribution of these species was also estimated from the beam intensity on the beam axis after the deflection by the SGIM.

In order to determine the effective magnetic field strength on the pole piece face of the magnetic hexapole, H_R, the velocity distribution and the spatial profile of the focused Rg* beam were measured under different magnetic hexapole lengths. The value of H_R was determined via a trajectory simulation fitting the experimental results.

2.2 Trajectory simulation of Rg* state-selection by the magnetic hexapole field

In the magnetic field $\mathbf{B}$, the Rg* atoms obey the so-called *Zeeman interaction Hamiltonian*, $\hat{H}'$ expressed by the following equation

$$\hat{H}' = -\boldsymbol{\mu}_J \cdot \mathbf{B}$$
$$\boldsymbol{\mu}_J = -g_J \frac{\mu_B}{\hbar}\mathbf{J} \tag{1}$$

where $\boldsymbol{\mu}_J$ is the magnetic moment of Rg* having the total angular momentum J, g_J is the g-factor of Rg* for the state with the total angular momentum of J, and μ_B is the Bohr magneton. Since Ar (^{3}P) and He (^{3}S) have no nuclear spin, there is no nuclear hyperfine interaction coupling to J. In this case, the Zeeman energy, W_{Zeeman}, follows from simple perturbation theory

$$W_{Zeeman} = \langle J\mathrm{M}_J|\,\hat{H}'\,|J\mathrm{M}_J\rangle = g_J\mu_B\mathrm{M}_J B \tag{2}$$

where M_J is the magnetic quantum number of J. Since the magnitude of the spin-orbit interaction of Ar ($^3P_2$) is much larger than the Zeeman interaction within the present magnetic field strength ($B < 0.4$ T), we need not consider the so-called "Paschen-Back effect" which occurs in the typical case of Ar ($^3P_2$) much larger magnetic field strength ($B > 10^3$ T). In our case, the g-factor can be simply expressed by the following equation based on the L-S coupling [11]

$$g_J = 1 + \frac{J(J+1) + S(S+1) - L(L+1)}{2J(J+1)} \tag{3}$$

where L is the total orbital angular momentum, S is the total spin angular momentum. Therefore, it is reasonable to use the linear model for the Zeeman diagram of Ar ($^3P_2$).

In the inhomogeneous magnetic hexapole field, Rg* atoms experience the radial force, Fr, expressed by the following equation;

$$Fr = -\frac{\partial W_{Zeeman}}{\partial r} = -g_J\mu_B\mathrm{M}_J\frac{\partial B(r)}{\partial r}$$
$$B(r) = \frac{H_R}{R^2}r^2 \tag{4}$$

where $B(r)$ is the magnetic field strength of the ideal magnetic hexapole at the radial distance r from the central

axis of the magnetic hexapole, H_R is the effective magnetic field strength on the pole piece face and R is the radial distance of the pole piece face from the central axis of the magnetic hexapole [12]. Since $g_J\mu_B$ has a positive value, the sign of Fr in equation (4) corresponds to the sign of $-M_J$. Therefore, focusing by the magnetic hexapole is possible when Rg* has the positive sign of M_J. In order to examine the performance of the magnetic hexapole, a numerical simulation of the state-selection was carried out. The radial force presented by equation (4) was applied for the trajectory simulation of the focusing behavior of Rg* in the magnetic hexapole field. In the simulation, an exact numerical calculation of the Rg* motion in the magnetic hexapole field was carried out point-by-point following Newton's equation. The motion of Rg* was calculated for the set of two parameters; v: the incident velocity, ϕ: the incident angle that is defined as the angle between the incident velocity and the hexapole central axis. The statistical weight of the incident angle is the distribution of the incident angle determined by the solid angle restricted by the geometrical parameters. The statistical weight of the velocity distribution was directly determined from the time-of-flight spectra of the direct beam. The geometrical factors are the hexapole radius and length as well as the collimator size and their location with respect to the beam source and detector. These geometrical factors are summarized in Figure 1. The effective magnetic field strength on the pole piece face, H_R, was used as a fitting parameter for the simulation. The successfully transmitted trajectories that have radial displacements within all collimator radii, have been summed up at the detector position as functions of velocity and spatial position. In this manner, the velocity distribution and the spatial distribution of the focused Rg* has been simulated.

3 Results and discussion

3.1 Effective magnetic field strength at the pole piece face

In order to determine the effective magnetic field strength on the pole piece face of the magnetic hexapole, (H_R), the velocity distributions of the focused He (^{3}S) beam were measured under different conditions of magnetic hexapole length. In this paper, such a velocity distribution is referred to as "focusing velocity curve (FVC)". Figure 2 shows the focusing velocity curves (FVC) of He (^{3}S) under the different condition of the magnetic hexapole length. As the hexapole length becomes short, a focused peak that was observed at the longer hexapole length moves toward the slower velocity region in the FVC at the shorter hexapole length. This is because the residence time of Rg* in the hexapole field becomes short. In addition, another peak appears in the faster velocity region as the hexapole length decreases. This result corresponds to the successive selection of the trajectories having lower number of oscillations in the magnetic hexapole field. At the hexapole length of 4 units, however, we can observe no

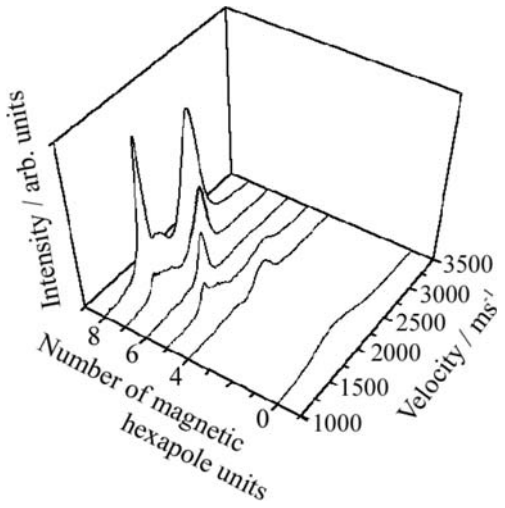

Fig. 2. The focusing velocity curves of He (^{3}S) in dependence upon the length of the magnetic hexapole field and together with the velocity distribution for the direct beam in the absence of the magnetic hexapole field.

appearance of another new peak in the faster velocity region. For this reason, we assign the focused peak appearing in the hexapole length of 4 units as the result of the trajectories that only experience 1/2 an oscillation in the magnetic hexapole field. Based on this assumption, a fitting parameter of H_R was determined by the simulation. The simulations using the parameter of $H_R = 0.4$ T nicely reproduce every FVC measured under different magnetic hexapole lengths. As a result, H_R is determined to be 0.4 T.

3.2 Characterization of focused Rg* beam

The velocity distribution and the spatial profile of the focused Rg* beam were measured using the position resolved time-of-flight method. Figure 3a shows the resultant 3D image of a He (^{3}S) beam focused by the 8 unit magnetic hexapole. Figure 3b is the simulated 3D image of the focused He (^{3}S) beam. Although the experimental 3D image turns out to be broadened as compared with the simulated one, the simulation nicely reproduces the slit position dependence and peak velocity of every focused peak in the experimental one. This broadening of the experimental 3D image might be due to imperfect alignment of the magnetic hexapole, and to deviation of the actual hexapole field from the ideal hexapole field by the multi-pole effect. It was found that the specified two velocities (around 1700 and 2300 ms^{-1}, which correspond to around 0.7 and 0.5 ms in the flight time, respectively) of the He (^{3}S) were selectively focused into two small spots (designated by peak 1 and peak 2) 60 cm downstream from the exit of the magnetic hexapole. The spatial profile at the focused peak 1 is shown in Figure 4a. The spot size of the focused He (^{3}S) beam was found to be 3 mm ϕ which is slightly wider than the simulated one (solid line). Significant enhancement of the beam intensity, up to one

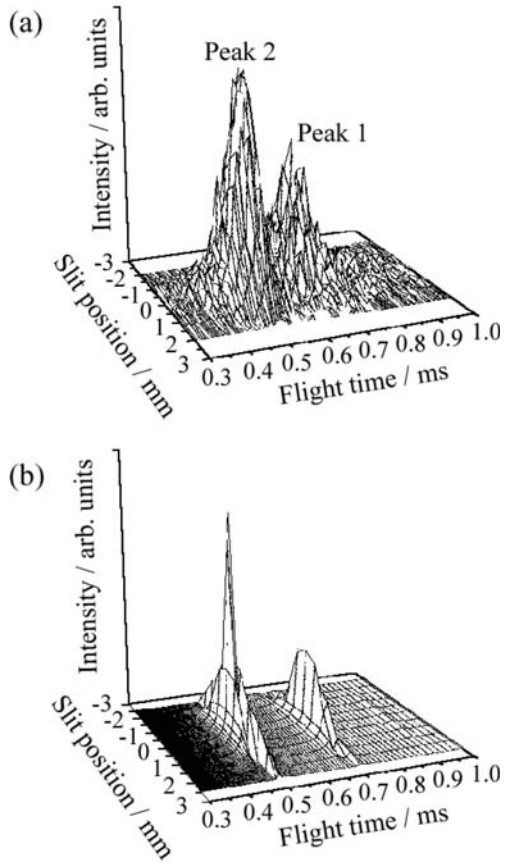

Fig. 3. 3D image of He (^{3}S) beam focused by the 8 units magnetic hexapole field; (a) experimental, (b) simulated.

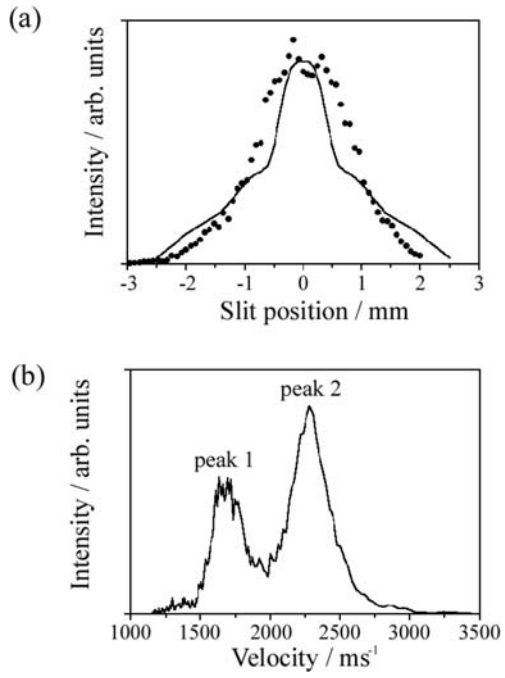

Fig. 4. (a) Spatial profile of the focused He (^{3}S) beam at the peak1; (•): experimental, (solid line): calculated from trajectory simulation. (b) Velocity distribution of the He (^{3}S) beam focused by the 8 units magnetic hexapole field.

order of magnitude, was observed as compared with that of the direct beam. The intensity of the focused He (^{3}S) beam was estimated to be 2.0×10^{17} atoms sr^{-1} s^{-1} at the peak 1. In addition, the velocity distribution for these two focused peaks is shown in Figure 4b. They were characterized as the translational temperature of 6.4 and 8.0 K, respectively. Since the velocity distribution of the direct beam is characterized as the translational temperature of 50 K, it was found that the magnetic hexapole field also acts as an excellent velocity selector.

3.3 Identification of the M_J state for the focused Rg* beam

For the application of the oriented Rg* beam to the advanced experimental studies on steric effects in gas phase and surface molecular reaction dynamics, it is important to know the M_J-state distribution of the state ensemble after the hexapole state-selection. In principle, the magnetic hexapole selectively focuses the Rg* with the positive sign of M_J. For example, for the He (^{3}S) beam, the $M_J = +1$ state is enhanced owing to the focusing effect, whereas, $M_J = -1$ state is efficiently removed by the defocusing effect and the $M_J = 0$ state (and He (^{1}S)) remains as the direct beam. In the present study, such M_J-state distribution was directly measured experimentally using the inhomogeneous magnetic field. For this purpose, the Stern-Gerlach type inhomogeneous magnet (SGIM) was set after the state selection by the magnetic hexapole. Figure 5a shows the 3D image of the focused He (^{3}S) beam after the deflection by the SGIM. The displacement becomes clear as the velocity becomes slow. In principle, although the randomly oriented He (^{3}S) beam is separated into three magnetic sub levels by the SGIM deflection, at a glance, it was found that the focused He (^{3}S) beam consists of two M_J-components. In other words, a complete removal of the $M_J = -1$ state by the magnetic hexapole is ascertained. The $M_J = +1$ component is found to consist of two peaks at the velocity regions around 1700 and 2300 ms^{-1}, just as observed in Figure 2. The efficient focusing of $M_J = +1$ component and the velocity selection by the magnetic hexapole were ascertained. As discussed in Section 3.1, these peaks correspond to the different two trajectory ensembles that experience different numbers of oscillation in the magnetic hexapole field. These focused peaks were nicely reproduced by the trajectory simulation. The typical trajectory in the magnetic hexapole field for each peak is shown in the right column in Figure 5. It was found that the $M_J = 0$ component (and He (^{1}S)) also coexist with the direct beam with the velocity distribution of the incident beam, although these components can be removed efficiently by the insertion of a beam stop if needed. In the same manner, we determined the M_J-state distribution of an Ar ($^3P_2$) beam after the hexapole state-selection. The 3D image of the focused Ar ($^3P_2$) beam after the deflection by the SGIM is shown in Figure 5b. The focused Ar ($^3P_2$) beam consists of three M_J-components. It was found that the magnetic hexapole completely removes the $M_J = -1$ and -2 states and the specific velocity

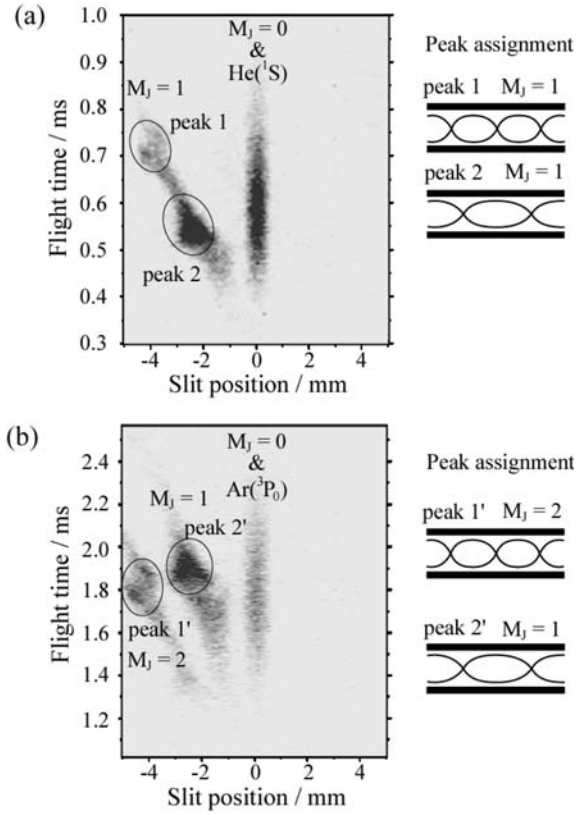

Fig. 5. 3D images of the time-of-flight spectra for the focused Rg* after the deflection by the Stern-Gerlach type inhomogeneous magnet (SGIM); (a) He (^{3}S), (b) Ar ($^3P_2$). "Peak assignment" column at the right side indicate the typical trajectory in the magnetic hexapole field for the corresponding peak.

regions were selectively focused for the $M_J = +1$ and $M_J = +2$ component respectively. Significant velocity selection by the magnetic hexapole was again ascertained. The trajectory simulation nicely reproduced every peak for the focused Ar ($^3P_2$) beam. The typical trajectory in the magnetic hexapole field assigned for each peak by the trajectory simulation is shown in the right column in Figure 5. The $M_J = 0$ component (and Ar ($^3P_0$)) also coexists as the direct beam with the velocity distribution of incident beam.

It was demonstrated that the newly developed oriented Rg* beam source based on the magnetic hexapole has a very excellent performance. It becomes feasible to study advanced stereodynamics by a combination of the oriented molecular beam and the oriented Rg* beam. Such a study is now in progress. The details will be reported elsewhere.

One of the authors, D. Watanabe, express his special thanks for the center of excellence (21COE) program "Creation of Integrated EcoChemistry" of Osaka University.

References

1. H. Ohoyama, T. Kasai, K. Ohashi, K. Kuwata, Chem. Phys. **165**, 155 (1992)
2. H. Ohoyama, T. Iguro, T. Kasai, K. Kuwata, Chem. Phys. Lett. **206**, 361 (1993)
3. H. Ohoyama, H. Makita, T. Kasai, K. Kuwata, J. Phys. Chem. **99**, 5798 (1995)
4. H. Ohoyama, R. Midorikawa, T. Kasai, J. Phys. Chem. A **101**, 7463 (1997)
5. S. Okada, H. Ohoyama, T. Kasai, J. Chem. Phys. **117**, 7925 (2002)
6. D. Watanabe, H. Ohoyama, M. Takahashi, T. Kasai, Eur. Phys. J. D (in press, 2006)
7. J. Baudon, F. Perales, C.H. Miniatura, J. Robert, G. Vassilev, J. Reinhardt, H. Harberland, Chem. Phys. **145**, 153 (1990)
8. W. Gerlach, O. Stern, Z. Phys. **9**, 349 (1922)
9. G.R. Woestenenk, J.W. Thomsen, M. van Rijnbach, P. van der Straten, A. Niehaus, Rev. Sci. Instrum. **72**, 3842 (2001)
10. A.P. Jardine, P. Fouquet, J. Ellis, W. Allison, Rev. Sci. Instrum. **72**, 3834 (2001)
11. P.F. Bernath, *Spectra of Atoms and Molecules* (Oxford University Press, New York, 1995)
12. G. Scoles, *Atomic and Molecular Beam Methods* (Oxford university Press, New York, 1988), Vol. 1, Chap. 11